Electronic Excitations of 1,4-Disilyl-Substituted 1,4-Disilabicycloalkanes: A MS-CASPT2 Study of the Influence of Cage Size

Niclas Sandström,[†] Mari Carmen Piqueras,[‡] Henrik Ottosson,*[,†] and Raül Crespo*[,‡]

Department of Biochemistry and Organic Chemistry, Box 576, Uppsala University, 751 23 Uppsala, Sweden, and Departament de Química Física, Universitat de València, Dr. Moliner 50, E-46100 Burjassot (Valencia), Spain

Received: January 2, 2007; In Final Form: February 8, 2007

We present a multistate complete active space second-order perturbation theory computational study aimed to predict the low-lying electronic excitations of four compounds that can be viewed as two disilane units connected through alkane bridges in a bicyclic cage. The analysis has focused on 1,4-disilyl-1,4-disilabicyclo-[2.2.1]heptane (**1a**), 1,4-*bis*(trimethylsilyl)-1,4-disilabicyclo[2.2.1]heptane (**1b**), 1,4-disilyl-1,4-disilabicyclo-[2.1.1]hexane (**2a**), and 1,4-*bis*(trimethylsilyl)-1,4-disilabicyclo[2.1.1]hexane (**2b**). The aim has been to find out the nature of the lowest excitations with significant oscillator strengths and to investigate how the cage size affects the excitation energies and the strengths of the transitions. Two different substituents on the terminal silicon atoms (H and CH_3) were used in order to investigate the end group effects. The calculations show that the lowest allowed excitations are of the same character as that found in disilanes but now red-shifted. As the cage size is reduced from a 1,4-disilabicyclo[2.2.1]heptane to a 1,4-disilabicyclo[2.1.1]hexane, the Si···Si through-space distance decreases from approximately 2.70 to 2.50 Å and the lowest allowed transitions are red-shifted by up to 0.9 eV, indicating increased interaction between the two Si−Si bonds. The first ionization potential, which corresponds to ionization from the Si−Si σ orbitals, is lower in **1b** and **2b** than in Si_2Me_6 by approximately 0.9 and 1.2 eV, respectively. Moreover, **1b** and **2b**, which have methyl substituents at the terminal Si atoms, have slightly lower excitation energies than the analogous species **1a** and **2a**.

Introduction

The spectroscopy and excited-state properties of linear peralkylated oligo- and polysilanes has been thoroughly investigated during the last few decades.[1,2] The general feature is that the optical and electronic properties of these systems are very dependent on the confirmation of the Si backbone,[3−8] and as a result, some polysilanes display thermo- and solvatochromism.[9] In an effort to identify alternative Si-based molecules that could display conjugative properties, yet be less conformationally flexible than oligosilanes, we investigated two different bicyclic structures: 1,4-disilabicyclo[2.2.1]heptane (**1**) and 1,4-disilabicyclo[2.1.1]hexane (**2**), substituted at the 1- and 4-positions by either silyl groups (**a**) or trimethylsilyl groups (**b**). These systems can be viewed as two disilane (disilyl) chromophores separated by three short alkyl chain tethers leading to bicyclic cage structures with Si atoms at the two bridgehead positions. The two bridgehead Si atoms are thereby in relatively close proximity to each other. We have previously computed the geometries and strain energies of the 1,3-disilabicyclo[1.1.1]pentane and 1,4-disilabicyclo[2.2.2]octane, as well as related systems, and found that these species are similarly or less strained than the all-carbon analogues,[10,11] which previously have been generated.[12,13] The compounds investigated herein should thus be realistic synthetic targets.

Previous spectroscopic and computational studies on substituted disilanes have shown that the first valence excitation is of Si−Si bond $\sigma-\pi^*$ character.[14] For disilanes with normal Si−Si bond lengths (∼2.35 Å), the first excitation energies measured at 77 K were found at 6.48 eV for hexamethyldisilane and at 6.27 eV for hexaethyldisilane. The second band, in cases where it could be observed, was found to have a polarization which was perpendicular relative to the first band, and thus, considered to be of Si−Si bond $\sigma-\sigma^*$ type. For hexaethyldisilane this peak was estimated at 6.7 eV, with roughly the same intensity as the first peak.

In our study the aim has been to predict the lowest valence excitations of two linked disilane molecules to clarify whether or not the proximity of the two Si−Si bonds affects the character and energies of these transitions, as well as to analyze the effect of the substituents at the terminal Si atoms. Previously, the multistate complete active space second-order perturbation theory (MS-CASPT2) technique has been shown to give accurate result and insight into the low-lying excitations of *n*-tetrasilane (*n*-Si_4H_{10})[15] and *n*-decamethyltetrasilane (*n*-Si_4Me_{10}).[16] It also provided a good description of the conformational dependence of the excitation energies and oscillator strengths, being in perfect accord with experimental results. The present investigation was therefore performed with the MS-CASPT2 method. The purpose of the investigation reported herein is to provide an accurate description of the nature of the lowest excitations that the 1,4-disilyl substituted 1,4-disilabicycloalkane cages display, and also to achieve an improved understanding of the Si−Si bond chromophore. Can the small disilabicycloalkane cages mediate interaction between the two Si−Si bonds, and how does such an interaction affect the excited states and their energies? Potentially, this could pave the way

* To whom correspondence should be addressed. E-mail: henrik.ottosson@biorg.uu.se (H.O.); raul.crespo@uv.es (R.C.).
[†] Uppsala University.
[‡] Universitat de València.

10.1021/jp070010n CCC: $37.00
Published on Web 03/17/2007

CHART 1

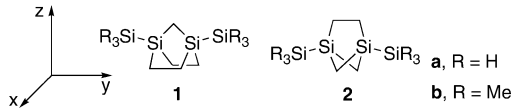

to design of novel Si-based molecular wires that display a new type of conjugation.

Computational Methods

Geometries. The geometries were first optimized at the DFT level using the B3LYP hybrid functional[17] and employing the 6-31G(d) double-ζ basis set.[18] The character of the stationary points was examined with frequency calculations performed at the same level of theory. All geometries were further optimized using second-order Møller-Plesset perturbation theory (MP2) with Dunning's correlation consistent triple-ζ basis set, cc-pVTZ,[19] for all atoms. All the calculations were performed within the C_{2v} symmetry point group constraints, with the *z*-axis as the twofold symmetry axis and the four silicon atoms lying in the *yz* plane. For molecules **1a** and **1b** the C atom of the methylene bridges, as well as the Si atoms, are in the *yz* plane. For molecules **2a** and **2b** it is the two C atoms of the ethylene bridge that lay in the *yz* plane (see Chart 1). All geometry optimizations were done with the Gaussian03 program package.[20]

Ring-Strain Energies. Ring-strain energies were obtained at the MP2/cc-pVTZ level according to a homodesmotic reaction scheme (see Supporting Information).[21] The calculations were done with the Gaussian03 program package.[20]

Electronic Excitation Energies. Electronic properties were computed from complete active space self-consistent field (CASSCF) wave functions employing a generally contracted basis set of atomic natural orbitals (ANOs) obtained from the Si(17s12p5d)/C(14s9p4d)/H(8s4p) primitive sets,[22] using the Si-[5s4p2d]/C[4s3p1d]/H[2s1p] contraction scheme. The reference wave function and the molecular orbitals were obtained from state average CASSCF calculations, where the averaging included all the A_1, B_2, A_2, and B_1 states of interest. The active space used in all the calculations was (4,4,2,2) where the numbers specify the number of active orbitals belonging to the a_1, b_2, a_2, and b_1 irreducible representations of the C_{2v} point group, respectively. The σ orbitals belong to the a_1 and b_2 irreducible representations of the C_{2v} point group, and the π orbitals belong to the a_2 and b_1 irreducible representations.

For **1a** and **1b** the active space for the occupied orbitals include one a_1 and one b_2 orbital, corresponding to the Si−Si bonds, one b_2 orbital corresponding to the bonds of the methylene bridge, and one a_2 and one b_1 orbital which correspond to the bonds of the ethylene bridges. The active space also included several virtual orbitals, three of a_1 symmetry, two of b_2 symmetry, one of a_2, and one of b_1 symmetry. The a_1 symmetry orbitals correspond to the Si−Si bonds, to the Si−methylene bridge bonds, and to the Si−H bonds (for **1a**) or Si−C bonds to the methyl groups (for **1b**). The b_2 orbitals correspond to the Si−methylene bridge bonds and to the Si−Si bond orbitals. The a_2 and b_1 symmetry orbitals correspond to the bonds in the methylene bridge and to the Si−H bonds (for **1a**) or Si−C bonds to the methyl groups (for **1b**).

The active space of **2a** and **2b** include each of the bonds in the methylene bridges (one a_1, one b_2, one a_2, and one b_1 symmetry orbitals) and also one b_2 symmetry orbital corresponding to the Si−Si bonds for the occupied part. The virtual orbitals include three a_1, two b_2, one a_2, and one b_1 symmetry orbitals. The three a_1 orbitals correspond to the Si−Si bonds, the orbital of the Si−methylene bridges (which are out of the molecular plane), and the C−H bonds of the methylene bridges. The b_2 orbitals correspond to the Si−methylene bridge (out of the plane) bonds and to the Si−Si bond orbitals. The a_2 and b_1 orbitals correspond to the interaction between the central Si atom and the methylene groups out of the plane. In all calculations the number of active electrons was set to ten.

To account for the remaining dynamic correlation, second-order perturbation theory with a multiconfigurational reference state, the CASPT2 approach,[23] was used. The CASPT2 method calculates the first-order wave function and the second-order energy with a CASSCF[24] wave function constituting the reference function. The coupling of the CASSCF wave functions via dynamic electron correlation was evaluated using the extended multistate CASPT2 (MS-CASPT2) method.[25] The MS-CASPT2 method showed very good agreement with experimental data for trisilane,[26] octamethyltrisilane,[27] *n*-tetrasilane,[15] and decamethyl-*n*-tetrasilane,[16] where state average CASSCF calculations introduce a strong mixing of Rydberg and valence states. The level shift technique handled any additional intruder states weakly interacting with the reference wave function.[28] A level shift of 0.15 has been used in all calculations in order to remove all intruder-state problems without affecting the excitation energies ($<$0.1 eV).

The CASSCF state interaction (CASSI) method[29] was employed to compute the transition dipole moments, which were combined with MS-CASPT2 energy differences to obtain oscillator strengths. The MS-CASPT2 oscillator strengths were obtained by use of the perturbation-modified CAS (PMCAS) reference functions,[25] obtained as linear combinations of all CAS states involved in the MS-CASPT2 calculation. These methods and techniques have been shown to work well for electronic excitation studies of oligosilanes. All MS-CASPT2 calculations were performed with the MOLCAS-6 quantum chemistry program.[30]

Ionization Potentials. The vertical ionization potentials were calculated at the HF/6-311G(d) level, applying Koopmans' theorem, at the MS-CASPT2 level, and also using the restricted outer valence Green's function electron propagator method (ROVGF)[31] with the 6-311G(d) basis set on the optimized MP2/cc-pVTZ geometries of the ground state. The HF and ROVGF calculations have been performed using the Gaussian03 program package[20] and the MS-CASPT2 calculations have been done with the MOLCAS-6 quantum chemistry program.[30]

Results

Geometries. Representative features of the MP2/cc-pVTZ optimized geometries calculated for **1a**, **1b**, **2a**, and **2b** molecules are shown in Figure 1. These geometries have been used in all computations of the electronic excitations.

DFT calculations using B3LYP/6-31G(d) gives C_{2v} symmetric structures as optimal for all systems. The geometrical parameters obtained at this level of theory are consistent with those obtained at the MP2/cc-pVTZ level. The values calculated at the MP2/cc-pVTZ (Figure 1) presumably represent the most reliable values available to date. For this reason, only the parameters obtained at this level of theory are included in Figure 1.

The values calculated for the Si−Si bonds in all four compounds (**1a**, **1b**, **2a**, and **2b**) are close to 2.35 Å (Figure 1), which is a normal bond distance in the disilane molecule, Si_2Me_6.[32] The optimized geometries obtained for the **1a** and **1b** molecules are very similar, and this is also the case for the geometries calculated for **2a** and **2b**. Hence, the change of the

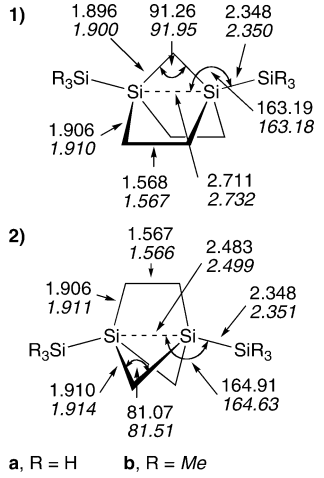

Figure 1. MP2/cc-pVTZ-optimized ground-state geometries of **1a**, **1b**, **2a**, and **2b**. Geometrical parameters of **1a** and **2a** are in normal print, and parameters of **1b** and **2b** are in italics. Bond lengths are in angstroms, and bond angles are in degrees.

end groups from silyl to trimethylsilyl has only an overall small effect on the geometrical parameters. The through-space Si···Si distances for type **1** systems are 2.71 (**1a**) and 2.73 (**1b**) Å. For type **2** cages, this distance shows values which are more than 0.2 Å shorter (2.48 and 2.50 Å for **2a** and **2b**, respectively). Thus, the through-space Si···Si distance of the cages is about 0.35 (for type **1**) and 0.15 Å (for type **2**) longer than a regular Si−Si single bond.

The C−C bond length values are close to 1.57 Å in all four structures while the geometries of the methylene bridges differ slightly between cages of type **1** and of type **2**. For compounds **1**, the Si−C bond length is 1.90 Å and the Si−C−Si bond angle is around 90°. For compounds **2**, the Si−C bond length shows similar values (1.91 Å); however, the value of the Si−C−Si bond angle decreases to approximately 80°. Consequently, the change from two ethylene bridges in type **1** to one ethylene bridge in type **2** disilabicycloalkanes, produces a major effect on the geometries of the cages.

Ring-Strain Energies. The calculated homodesmotic ring strain energies for **1a** and **1b** molecules are 15.9 and 15.7 kcal/mol, respectively. For **2a** and **2b** molecules, with one shorter carbon bridge and shorter Si···Si through-space distances, the ring strain energies are 29.6 and 28.6 kcal/mol, respectively. Thus, the ring strain is not affected by the change of the end groups from silyl (**1a** and **2a**) to trimethylsilyl (**1b** and **2b**). However, the change from two ethylene bridges (**1a** and **1b**) to just one (**2a** and **2b**) leads to an increase of the ring strain by approximately 14 kcal/mol.

Ionization Potentials (IPs). The first five vertical IP calculated at the MS-CASPT2, ROVGF/6-311G(d), and HF/6-311G(d) level (Koopmans' theorem) for the **1a**, **1b**, **2a**, and **2b** molecules are collected in Table 1. The values calculated at the MS-CASPT2 and at the ROVGF level are very similar for all the systems. The largest differences between the two methodologies are about 0.3 eV. As can be expected, the values obtained at the HF level show rather large deviations when compared to both MS-CASPT2 and ROVGF calculated values.

For compound **1a**, the 1^2B_2 and 1^2A_2 states are almost degenerated in energy at the MS-CASPT2 (8.80 and 8.75 eV, respectively) and ROVGF (8.82 and 8.84 eV, respectively) levels of theory. Replacing the H atoms at Si (**1a** and **2a**) with Me groups (**1b** and **2b**) makes the 1^2B_2, 2^2A_2, and 1^2B_1 (only in type **1** cages) states shift to lower energies by about 1.0 eV. This is not surprising as it is a very local effect on the Si−Si bond. The other states display a decrease of about 0.5 eV.

The change of one methylene to two methylene bridges (going from cages of type **1** to cages of type **2**) gives a slightly smaller change of the IP values, of about 0.4 eV, except for the 1^2B_1 states (9.93 and 9.95 eV for **1b** and **2b**, respectively). Interestingly, the 1^2A_2 and 2^2A_2 states display increases of 0.3−0.5 eV when going from systems **1** to **2**.

Electronic Excitations of 1a and 1b. Table 3 displays the main configurations (contributions of more than 10%) and the weights of the wave function of the lowest excited states of **1a**, **1b**, **2a**, and **2b**. All molecules have a nearly single determinant ground state but many of the low-lying valence excited states investigated in this study show a strong multiconfigurational character. The MS-CASPT2 vertical excitation energies calculated for **1a** and **1b** are shown in Table 2. The ionization energies according to MS-CASPT2 and ROVGF calculations are around 8.8 eV for **1a**, and around 7.9 eV for **1b**. Therefore, we list only states with excitation energies around 7.0 (**1a**) and 6.3 (**1b**) eV, in order to include the same number of states of each symmetry class for both systems. Consequently, the electronic transitions include four B_2 states, three A_2 states, two A_1 states, and two B_1 excited states. As written in the computational methods section, the σ and σ^* orbitals belong to the a_1 and b_2 irreducible representations of the C_{2v} symmetry point group, and the π and π^* orbitals to the a_2 and b_1 irreducible representations. The main configurations of the transitions and their percentual weights are listed in Table 3.

We first focus on the electronic excitations of molecule **1a**. The dipole-allowed vertical electronic transitions are located in two intervals, at about 6.0 and 6.5 eV, respectively. The first band is mainly due to the lowest energy transition, which lies at 6.00 eV, and it is to the 1^1B_2 state. This electronic transition ($\sigma-\sigma^*$) shows the strongest oscillator strength (0.39) calculated for this molecule. At an almost degenerate energy to the first excitation there is a symmetry forbidden transition to the 1^1A_2 state (6.01 eV), which corresponds to a $\pi-\sigma^*$ electronic transition. The transition to the 2^1A_1 state ($\pi-\pi^*$) lies at 6.20 eV and shows a rather low oscillator strength (0.08). It is also almost isoenergetic with a symmetry forbidden transition to the 2^1A_2 ($\pi-\sigma^*$) state (6.24 eV). The second band of **1a** is located at around 6.5 eV, and it includes five different excitations, all of them very close in energy lying from 6.39 to 6.61 eV. The first transition is to the 1^1B_1 ($\pi-\sigma^*$) state, located at 6.39 eV, and has small oscillator strength (0.08). The transitions to the 2^1B_2 ($\sigma-\sigma^*$) and to the 3^1A_1 ($\sigma-\sigma^*$) states show larger oscillator strengths (0.15 and 0.18, respectively), being the second strongest electronic transitions for this system. The next transition, to the 3^1B_2 ($\sigma-\sigma^*$) state (6.58 eV), presents an oscillator strength that is similar to the first one (0.07). The last state contributing to this band is the 2^1B_1 ($\sigma-\pi^*$) state, located at 6.61 eV, which shows a larger value of the oscillator strength (0.13). The last two states, the 3^1A_2 ($\sigma-\pi^*$) state at 6.75 eV and the 4^1B_2 ($\sigma-\sigma^*$) state at 6.99 eV, do not show a strong effect on the spectrum, as the first one is forbidden by symmetry and the second one presents a small value of the oscillator strength (0.06).

Replacing the H atoms of the silyl groups by methyl groups, leading to molecule **1b**, results in a spectrum which also shows two intervals, but now they are located at about 5.5 and 6.2 eV, respectively. The first band is mainly due to the first electronic transition located at 5.51 eV. This electronic transition is also to the 1^1B_2 state ($\sigma-\sigma^*$), and it also shows the strongest oscillator strength (0.35). The next transition, the excitation to

TABLE 1: Calculated MS-CASPT2 and ROVGF Ionization Potentials (eV) of 1a, 1b, 2a, and 2b

	1a		1b		2a		2b	
state	MS-CASPT2	ROVGF[a,b]	MS-CASPT2	ROVGF[a,b]	MS-CASPT2	ROVGF[a,b]	MS-CASPT2	ROVGF[a,b]
1^2B_2	8.80	8.82 (9.83)	7.81	7.91 (9.06)	8.42	8.45 (9.40)	7.48	7.57 (8.65)
2^2B_2	9.31	9.35 (10.55)	8.83	8.91 (10.16)	8.88	9.15 (10.28)	8.34	8.66 (9.85)
1^2A_2	8.75	8.84 (10.05)	8.32	8.43 (9.68)	9.27	9.35 (10.42)	8.82	8.92 (10.05)
2^2A_2	9.41	9.66 (10.73)	8.56	8.79 (9.97)	9.70	10.04 (11.15)	8.88	9.21 (10.41)
1^2B_1	10.76	10.79 (12.15)	9.93	10.19 (11.54)	10.42	10.49 (11.87)	9.95	10.02 (11.42)

[a] Calculated at ROVGF/6-311G(d)//MP2/cc-pVTZ level. [b] In parenthesis, IP calculated according to Koopmans' theorem at the HF/6-311G(d)//MP2/cc-pVTZ level.

TABLE 2: MS-CASPT2 Vertical Excitation Energies (*E*, eV) and Oscillator Strengths (*f*) of 1a and 1b

1a			1b		
state	*E* (eV)	*f*	state	*E* (eV)	*f*
1^1B_2	6.00	0.39	1^1B_2	5.51	0.35
1^1A_2	6.01	0[a]	1^1A_2	5.78	0[a]
2^1A_1	6.20	0.08	2^1B_2	5.92	0.10
2^1A_2	6.24	0[a]	2^1A_2	5.95	0[a]
1^1B_1	6.39	0.08	2^1A_1	5.97	0.06
2^1B_2	6.45	0.15	3^1B_2	6.07	0.02
3^1A_1	6.50	0.18	1^1B_1	6.09	0.11
3^1B_2	6.58	0.07	3^1A_2	6.09	0[a]
2^1B_1	6.61	0.13	3^1A_1	6.19	0.12
3^1A_2	6.75	0[a]	2^1B_1	6.27	0.01
4^1B_2	6.99	0.06	4^1B_2	6.33	0.19

[a] Transitions forbidden by symmetry.

the dark 1^1A_2 state ($\pi-\sigma^*$) is located at 5.78 eV. The second band is due to all the other calculated excited states. The strongest contributions come from the 2^1B_2 ($\sigma-\sigma^*$) state located at 5.92 eV, from the 1^1B_1 ($\sigma-\pi^*$) state located at 6.09 eV, from the 3^1A_1 ($\sigma-\sigma^*$) state located at 6.19 eV, and from the 4^1B_2 ($\sigma-\sigma^*$) state located at 6.33 eV. All of them show similar oscillator strengths, of about 0.10, except the 4^1B_2 state, which shows a larger value of 0.19.

Related to the effect of the methyl substitution on the excited states, all the $^1B_2$ symmetry states of **1b** (from 1^1B_2 to 4^1B_2) present a similar behavior as they also show a decrease in the energy of about 0.5 eV when compared to the values calculated for the **1a** molecule. For all the other states of **1b**, except for the 3^1A_2 ($\sigma-\pi^*$) state, a smaller decrease in the energies, of about 0.3 eV, are observed when compared to the values obtained for **1a**. The 3^1A_2 state is the one that presents a large decrease of the energy (about 0.7 eV) with respect to the value calculated for this state in **1a**. The oscillator strengths calculated for the states of **1b** show values rather similar to those calculated for **1a**, except for the 2^1B_1 ($\pi-\sigma^*$) and 4^1B_2 states which are almost degenerate in energy in molecule **1b** and have values of the oscillator strengths that are somewhat different to those of **1a**.

Electronic Excitations of 2a and 2b. The MS-CASPT2 vertical excitation energies calculated for **2a** and **2b** are shown in Table 4. The ionization energies according to MS-CASPT2 and ROVGF calculations are around 8.5 eV for **2a** and around 7.6 eV for **2b**. Therefore, we list only states with excitation energies around 6.9 (**2a**) and 6.1 (**2b**) eV, in order to include the same number of states of each symmetry class for both systems. Thus, the electronic transitions include four B_2 states, two A_2 states, two A_1 states, and one B_1 excited states.

The dipole-allowed vertical transitions that have significant intensity for **2a** are all of B_2 and A_1 symmetry, and they are located in two well-defined regions at about 5.8 and 6.4 eV. The lowest two excitations of **2a** are both dark transitions into states of A_2 ($\sigma-\pi^*$) symmetry, located at 5.10 and 5.74 eV, respectively, and therefore, they have no contribution to the first band. As a consequence, the first allowed transition, which is also into the 1^1B_2 state (as found for **1a** and **1b**), is located at 5.81 eV, and it shows a very strong oscillator strength (0.77). This state corresponds mainly to a $\sigma-\sigma^*$ electronic transition. There is also a contribution to this first band from two other states, the 2^1B_2 state ($\pi-\pi^*$) located at 6.00 eV and which shows a significant value of the oscillator strength (0.16), and the 2^1A_1 ($\sigma-\sigma^*$) state at 6.13 eV and which has a smaller oscillator strength (0.07). The next two states, 3^1B_2 ($\sigma-\sigma^*$) and 4^1B_2 ($\sigma-\sigma^*$), show almost negligible oscillator strengths. The next band of **2a** is located at about 6.6 eV, and it is due to the contributions from the 3^1A_1 ($\sigma-\sigma^*$) and 1^1B_1 states ($\pi-\sigma^*$), which have oscillator strengths of 0.12 and 0.08, respectively.

For the methyl-substituted system **2b**, the excitations are also located in two regions, around 5.4 and 5.8 eV, respectively, and the strongest excitations are to B_2 and B_1 symmetric states. The electronic excitations calculated for molecule **2b** show that, similar as for **2a**, the first transition is to the symmetry forbidden 1^1A_2 ($\sigma-\pi^*$) state located at 4.76 eV (0.34 eV lower in energy than that calculated for **2a**). The first band is due to the second lowest excitation, which is into the 1^1B_2 state ($\sigma-\sigma^*$). This state lies at 5.4 eV and the transition has rather strong oscillator strength (0.25). The second band appears at about 5.8 eV, and it is mainly due to the excitation to the 2^1B_2 state ($\pi-\pi^*$), which displays the strongest oscillator strength (0.45) of all transitions in **2b**. The second band also has very small contributions from the 2^1A_1 ($\sigma-\sigma^*$) state (0.05) and from the 3^1B_2 ($\sigma-\sigma^*$) state (0.03). The 2^1A_2 ($\sigma-\pi^*$) state is also located in this region (5.68 eV); however, it does not contribute to the band since it corresponds to a symmetry-forbidden electronic transition. The next band is located at about 6.0 eV, and it is mainly due to the 1^1B_1 state ($\sigma-\pi^*$) found at 6.01 eV, which shows an oscillator strength of 0.15. The other two states, 3^1A_1 ($\sigma-\sigma^*$) and 4^1B_2 ($\sigma-\sigma^*$), show smaller contributions to this band.

Discussion

Geometries and Ring Strain. The largest geometric difference between the two types of disilabicycloalkane cages, **1** and **2**, is the Si···Si through-space distance. By changing from two ethylene bridges in **1** to one ethylene bridge in **2**, the Si···Si through-space distance decreases from about 2.70 to about 2.50 Å. This makes the methylene Si−C−Si bond angle close by approximately 10° and also that the Si−C bonds of the methylene bridges stretch slightly. However, changing the end groups from silyl to trimethylsilyl has nearly no effect on the geometrical parameters of the disilabicycloalkane cages and the Si−Si single bond lengths.

With regard to the ring strain, it increases by approximately 14 kcal/mol when going from **1** to **2**, but the strain of **2** (28−30 kcal/mol) is still not so high that it will prevent the synthetic realization of this compound. It is noteworthy that Kira and co-workers recently formed a substituted 1,3-disilabicyclo[1.1.0]-

TABLE 3: Main Configurations (>10%) and Weights (%) for the Lowest Excited States of 1a, 1b, 2a, and 2b[a]

1a			1b			2a			2b		
state	configuration	*W* (%)	state	configuration	*W* (%)	state	configuration	*W* (%)	state	configuration	*W* (%)
1^1A_1	Hartree−Fock	98	1^1A_1	Hartree−Fock	98	1^1A_1	Hartree−Fock	96	1^1A_1	Hartree−Fock	97
2^1A_1	$7a_2\rightarrow 8a_2^*$	90	2^1A_1	$23b_2\rightarrow 24b_2^*$	79	2^1A_1	$15b_2\rightarrow 16b_2^*$	78	2^1A_1	$22b_2\rightarrow 23b_2^*$	71
							$14b_2\rightarrow 16b_2^*$	14		$22b_2\rightarrow 24b_2^*$	15
3^1A_1	$16b_2\rightarrow 17b_2^*$	36	3^1A_1	$26a_1\rightarrow 27a_1^*$	45	3^1A_1	$14b_2\rightarrow 16b_2^*$	80	3^1A_1	$22b_2\rightarrow 24b_2^*$	69
	$16b_2\rightarrow 18b_2^*$	22		$22b_2\rightarrow 25b_2^*$	33		$15b_2\rightarrow 16b_2^*$	14		$22b_2\rightarrow 23b_2^*$	15
	$15b_2\rightarrow 17b_2^*$	18		$26a_1\rightarrow 28a_1^*$	11						
	$19a_1\rightarrow 20a_1^*$	13									
1^1B_2	$16b_2\rightarrow 20a_1^*$	50	1^1B_2	$23b_2\rightarrow 27a_1^*$	58	1^1B_2	$15b_2\rightarrow 20a_1^*$	60	1^1B_2	$22b_2\rightarrow 27a_1^*$	48
	$15b_2\rightarrow 20a_1^*$	34		$23b_2\rightarrow 29a_1^*$	21		$15b_2\rightarrow 22a_1^*$	15		$21b_2\rightarrow 27a_1^*$	30
							$5a_2\rightarrow 9b_1^*$	10			
2^1B_2	$15b_2\rightarrow 20a_1^*$	39	2^1B_2	$23b_2\rightarrow 28a_1^*$	48	2^1B_2	$5a_2\rightarrow 9b_1^*$	75	2^1B_2	$10a_2\rightarrow 14b_1^*$	81
	$16b_2\rightarrow 20a_1^*$	34		$22b_2\rightarrow 28a_1^*$	29						
	$15b_2\rightarrow 21a_1^*$	18									
3^1B_2	$16b_2\rightarrow 21a_1^*$	52	3^1B_2	$12a_2\rightarrow 15b_1^*$	84	3^1B_2	$15b_2\rightarrow 21a_1^*$	61	3^1B_2	$22b_2\rightarrow 28a_1^*$	43
	$16b_2\rightarrow 22a_1^*$	14					$15b_2\rightarrow 20a_1^*$	15		$22b_2\rightarrow 29a_1^*$	23
	$15b_2\rightarrow 21a_1^*$	12					$15b_2\rightarrow 22a_1^*$	14		$21b_2\rightarrow 28a_1^*$	18
4^1B_2	$15b_2\rightarrow 22a_1^*$	54	4^1B_2	$22b_2\rightarrow 27a_1^*$	63	4^1B_2	$14b_2\rightarrow 20a_1^*$	86	4^1B_2	$21b_2\rightarrow 27a_1^*$	49
	$16b_2\rightarrow 21a_1^*$	23		$23b_2\rightarrow 29a_1^*$	23					$22b_2\rightarrow 27a_1^*$	28
	$15b_2\rightarrow 20a_1^*$	10									
1^1A_2	$7a_2\rightarrow 20a_1^*$	86	1^1A_2	$12a_2\rightarrow 27a_1^*$	69	1^1A_2	$15b_2\rightarrow 9b_1^*$	75	1^1A_2	$22b_2\rightarrow 14b_1^*$	64
				$12a_2\rightarrow 28a_1^*$	25		$14b_2\rightarrow 9b_1^*$	15		$21b_2\rightarrow 14b_1^*$	27
2^1A_2	$7a_2\rightarrow 21a_1^*$	58	2^1A_2	$12a_2\rightarrow 28a_1^*$	41	2^1A_2	$14b_2\rightarrow 9b_1^*$	76	2^1A_2	$21b_2\rightarrow 14b_1^*$	64
	$7a_2\rightarrow 22a_1^*$	34		$12a_2\rightarrow 27a_1^*$	38		$15b_2\rightarrow 9b_1^*$	16		$22b_2\rightarrow 14b_1^*$	27
3^1A_2	$16b_2\rightarrow 10b_1^*$	48	3^1A_2	$23b_2\rightarrow 15b_1^*$	57						
	$19a_1\rightarrow 8a_2^*$	39		$22b_2\rightarrow 15b_1^*$	23						
1^1B_1	$7a_2\rightarrow 17b_2^*$	73	1^1B_1	$23b_2\rightarrow 13a_2^*$	47	1^1B_1	$5a_2\rightarrow 16b_2^*$	65	1^1B_1	$26a_1\rightarrow 14b_1^*$	80
	$7a_2\rightarrow 18b_2^*$	17		$22b_2\rightarrow 13a_2^*$	40		$5a_2\rightarrow 17b_2^*$	30		$22b_2\rightarrow 11a_2^*$	10
2^1B_1	$16b_2\rightarrow 8a_2^*$	54	2^1B_1	$12a_2\rightarrow 24b_2^*$	79						
	$15b_2\rightarrow 8a_2^*$	35		$12a_2\rightarrow 25b_2^*$	11						

[a] The HOMO is orbital $16b_2$ (**1a**), $23b_2$ (**1b**), $15b_2$ (**2a**), and $22b_2$ (**2b**).

TABLE 4: MS-CASPT2 Vertical Excitation Energies (*E*, eV) and Oscillator Strengths (*f*) of 2a and 2b

2a			2b		
state	*E* (eV)	*f*	state	*E* (eV)	*f*
1^1A_2	5.10	0[a]	1^1A_2	4.76	0[a]
2^1A_2	5.74	0[a]	1^1B_2	5.37	0.25
1^1B_2	5.81	0.77	2^1A_1	5.56	0.05
2^1B_2	6.00	0.16	2^1A_2	5.68	0[a]
2^1A_1	6.13	0.07	2^1B_2	5.69	0.45
3^1B_2	6.23	0.01	3^1B_2	5.74	0.03
4^1B_2	6.38	0.03	1^1B_1	6.01	0.15
3^1A_1	6.41	0.12	3^1A_1	6.08	0.03
1^1B_1	6.88	0.08	4^1B_2	6.11	0.02

[a] Transitions forbidden by symmetry.

butane which is thermally stable until its melting point at 170−175 °C.[33] For the parent 1,3-disilabicyclo[1.1.0]butane, we previously calculated a strain energy of 63.9 kcal/mol at MP2/6-31G(d) level.[10]

IPs. The reduction of the IP with methyl substitution (in going from **1a** to **1b** and from **2a** to **2b**) cannot be related to the changes in the Si−Si bond or Si···Si through-space distances (from 2.71 Å in **1a** to 2.73 Å in **1b** and from 2.48 Å in **2a** to 2.50 Å in **2b**). We attribute the first IP to the removal of an electron from the σ_{SiSi} orbital (highest-occupied molecular orbital, HOMO) in agreement with that observed for other disilanes.[14] The general decrease in this IP with increasing the size of the substituent (from H to methyl group) can thus be attributed to the stabilization of the radical cation by the increasing polarizable bulk (substituent inductive effect).

More important are, however, the change in the first IPs that occur upon reducing the size of the cages from **1** to **2** as this reflects the extent of interaction between the two Si−Si bonds through the cages. For the unsubstituted systems the decrease in the first IP is 0.38 and 0.37 eV at MS-CASPT2 and ROVGF levels, respectively. And for the methyl substituted systems **1b** and **2b** the corresponding lowerings are 0.33 and 0.34 eV, respectively. Considering that the two pairs **1a**/**2a** and **1b**/**2b** only differ in size by a CH_2 unit, this reduction is substantial and should stem from the shortening in Si···Si through-space distance by ∼0.2 Å. Moreover, if the two Si−Si bonds in **1b** and **2b** were not interacting the first IPs should resemble that of Si_2Me_6 (8.7 eV);[14] however, their IPs are lower by 0.9 and 1.2 eV, respectively. Interestingly, the value calculated for the first IPs of **1b** and **2b** are even lower than the value obtained for $Si_2(t\text{-}Bu)_6$ (8.1 eV),[14] a molecule with a Si−Si bond length of 2.686 Å,[34] i.e., ∼0.35 Å longer than normal Si−Si bond lengths,[35] and as a consequence a particularly low IP. It should be noted that the Si−Si bonds in each of **1** and **2** are of regular lengths.

Electronic Excitations. By comparison of **1a** to **1b** it can be noted that both systems have the lowest transition to the 1^1B_2 state and that this transition also has the strongest oscillator strength. The transition of the methyl-substituted compound is red-shifted by 0.5 eV compared to the hydrogen-substituted one. This transition is of $\sigma-\sigma^*$ character, and the major contribution is from an excitation out of the HOMO (Table 3). For **1a** the near degeneracy of the 1^1B_2 and the 1^1A_2 states at 6.0 eV correlates with the very small difference in energy seen in the ionization potentials for this system. This is not the case in **1b** where the hydrogens are substituted to methyl groups. Now the 1^1B_2 state is separated from the 1^1A_2 state by 0.3 eV, although the transitions are of the same character as in **1a**, $\sigma-\sigma^*$ and $\pi-\sigma^*$ type, respectively. With regard to the transitions with medium oscillator strengths, they all have contributions from excitations out of the HOMO; the 2^1B_2, 3^1A_1, and 2^1B_1 states in **1a** and the 2^1B_2, 1^1B_1, and 4^1B_2 states in **1b** (Table 3).

Besides the red-shift of the energies of all states with methyl substitution, stressed in the results section, the main differences between **1a** and **1b** are seen in the character of the 2^1A_1, 3^1B_2, 1^1B_1, and 2^1B_1 states. While the 2^1A_1 state is a $\pi-\pi^*$ transition in **1a**, it corresponds to a $\sigma-\sigma^*$ transition in **1b**. For the 3^1B_2 state, the opposite is the case, as it is a $\sigma-\sigma^*$ transition in **1a** and a $\pi-\pi^*$ transition in **1b**. The character of the 1^1B_1 and 2^1B_1 states is exchanged in both compounds, since in **1a** they are of $\pi-\sigma^*$ and of $\sigma-\pi^*$ character, respectively, whereas in **1b** they are of $\sigma-\pi^*$ and $\pi-\sigma^*$ type, respectively. In summary, the change from hydrogen to methyl substituents at the terminal Si atoms red-shifts the excitations of **1** with an average of 0.42 eV with the exception of excitations where the high-energy $7a_2$ orbital, which is a π_{SiC} orbital located in the ethylene bridges, have a large influence, in which case the red-shift is decreased by up to 0.2 eV.

Upon changing the hydrogens on the terminal Si atoms to methyl groups in systems **2**, i.e., going from **2a** to **2b**, one can note an overall larger similarity of the transitions between these two systems than for molecules **1a** and **1b**. Both **2a** and **2b** have the lowest allowed transition to the 1^1B_2 state, and this transition has the strongest oscillator strength for **2a** and the second strongest value for **2b**. The 1^1B_2 transition of the methyl-substituted compound is red-shifted by 0.5 eV compared to the hydrogen substituted one. This transition is of $\sigma-\sigma^*$ character and the major contribution is from the excitation out of HOMO (Table 3). The transitions to the 2^1B_2 states, on the other hand, are in both compounds of $\pi-\pi^*$ type, and these excitations show medium (**2a**) and strong (**2b**) oscillator strengths, respectively. With regard to the forbidden excitations to the A_2 states, which are the two lowest transitions in **2a** and first and fourth in **2b**, they are both from the HOMO. As it was shown in compounds **1a** and **1b**, the character of the B_1 states is exchanged in both compounds, because in **2a** it presents $\pi-\sigma^*$ character and in **2b** it is of $\sigma-\pi^*$ type. Furthermore, the red-shift upon methyl substitution at the terminal Si atoms of **2** is similar to that found for systems **1**, with an average 0.41 eV with a few exceptions. With regard to the oscillator strength, the methylated terminal Si atoms favor excitations with $\pi\rightarrow\pi^*$ character over $\sigma\rightarrow\sigma^*$ character.

By comparison of 1,4-disila-substituted 1,4-disilabicycloalkanes of types **1** and **2**, one can see that the 2^1A_1 state is of $\sigma-\sigma^*$ character, except in compound **1a** where it is of $\pi-\pi^*$ type. For the B_2 states, all systems present three states that are of $\sigma-\sigma^*$ character and one state that is of $\pi-\pi^*$ character, except for **1a** where all four states are of $\sigma-\sigma^*$ type. The two A_2 states present $\pi-\sigma^*$ character for type **1** bicycloalkanes and they are of $\sigma-\pi^*$ character for type **2** bicycloalkanes.

When comparing **1a** and **1b** to **2a** and **2b**, respectively, the lowest excitation is 0.8−0.9 eV red-shifted in the latter two compounds, whereas if one compares the lowest dipole-allowed transition the difference is smaller, only 0.1−0.2 eV. However, in all four compounds the very lowest excitation involves the methylene bridges, although this excitation in **1a** and **1b** is of $\sigma-\sigma^*$ character (1^1B_2) and in **2a** and **2b** it is of $\sigma-\pi^*$ character (1^1A_2). This change in character stems from the fact that in **1a** and **1b** the methylene bridge is in the symmetry plane along the long-axis of the molecule, the *yz* plane, whereas in **2a** and **2b** the two methylene bridges are above and below this plane, respectively. However, in all four compounds the lowest excitations involve configurations in which one electron is promoted from HOMO to an orbital located on the methylene bridges. Because of the location of the methylene bridges in-plane and out-of-plane, respectively, this transition is symmetry allowed in **1a** and **1b** whereas it is symmetry forbidden in **2a** and **2b**. But as judged from the character the transition can in both compound types be described as an excitation involving the methylene bridge(s), and interestingly, this transition is red-shifted by nearly 1 eV when going from **1** to **2**, a strong indicator of improved Si−Si bond interaction as the tethers in the bicyclic compound are made shorter.

Conclusion and Outlook

The photophysical properties of short oligosilanes are well studied, and effects of conformation on observed spectra can be explained rationally. These conformational changes are also the reason why the σ-conjugation in oligosilanes can be attenuated and even broken.[6] The systems we have investigated in this study are potential building blocks for a more rigid oligomer with a backbone of Si−Si bonds and carbon cage structures. The lowest excited state is not of the same character as in oligosilanes due to the bicycloalkane cage structure separating the Si−Si bonds; instead, it is rather similar to that of disilane. As the cage introduces an interaction between the two Si−Si bonds, there is a red-shift in the lowest valence excitations. The red-shift is largest for the smallest cage, 1,4-disilabicyclo[2.1.1]hexane, which has the shortest through-space Si···Si distance. After having observed the effect of the methylene bridge in reducing the Si···Si through-space distance and red-shifting the electronic transitions, we reason that the 1,3-disilabicyclo[1.1.1]pentane cage should display very interesting electronic properties since it provides an even shorter Si···Si through-space distance and presumably the strongest coupling between the two Si−Si bonds and the bicycloalkane cage.

Acknowledgment. N.S. and H.O. are grateful to the Swedish research council (Vetenskapsrådet) for financial support and the Liljewalchs foundation for a travel grant to N.S. that enabled a secondment at University of Valencia. R.C. and M.C.P. are grateful to Universitat de València, Generalitat Valenciana, Ministerio de Educación y Ciencia, Ministerio de Medio Ambiente and the European Commission for financial support.

Supporting Information Available: Homodesmotic reaction schemes, absolute energies, and Cartesian coordinates. This material is available free of charge via the Internet at http://pubs.acs.org.

References and Notes

(1) Miller, R. D.; Michl, J. *Chem. Rev.* **1989**, *89*, 1359.

(2) Michl, J.; West, R. In *Silicon Based Polymers: The Science and Technology of their Synthesis and Applications*; Jones, R. G., Ando, W., Chojnowski, J., Eds.; Kluwer Academic Publishers: Dordrecht, The Netherlands, 2000; pp 499 − 529.

(3) (a) Albinsson, B.; Teramae, H.; Downing, J. W.; Michl, J. *Chem.−Eur. J.* **1996**, *2*, 529. (b) Albinsson, B.; Antic, D.; Neumann, F.; Michl, J. *J. Phys. Chem. A* **1999**, *103*, 2184. (c) Ottosson, C.-H.; Michl, J. *J. Phys. Chem. A* **2000**, *104*, 3367. (d) Fogarty, H. F.; Ottosson, H.; Michl, J. *J. Phys. Chem. B* **2006**, *110*, 25485.

(4) (a) Fukazawa, A.; Tsuji, H.; Tamao, H. *J. Am. Chem. Soc.* **2006**, *128*, 6800. (b) Tsuji, H.; Terada, M.; Toshimitsu, A.; Tamao, K. *J. Am. Chem. Soc.* **2003**, *125*, 7486. (c) Tsuji, H.; Fukazawa, A.; Yamaguchi, S.; Toshimitsu, A.; Tamao, K. *Organometallics* **2004**, *23*, 3375. (d) Mallesha, H.; Tsuji, H.; Tamao, K. *Organometallics* **2004**, *23*, 1639.

(5) Fogarty, H. A.; Tsuji, H.; David, D. E.; Ottosson, C.-H.; Ehara, M.; Nakatsuji, H.; Tamao, K.; Michl, J. *J. Phys. Chem. A* **2002**, *106*, 2369.

(6) Tsuji, H.; Toshimitsu, A.; Tamao, K.; Michl, J. *J. Phys. Chem. A* **2001**, *105*, 10246.

(7) Okumura, H.; Kawaguchi, A.; Harada, A. *Macromol. Rapid Commun.* **2002**, *23*, 781.

(8) (a) Sakamoto, K.; Naruoka, T.; Kira, M. *Chem. Lett.* **2003**, *32*, 380. (b) Sanji, T.; Yoshiwara, A.; Sakurai, H.; Tanaka, M. *Chem. Commun.* **2003**, 1506.

(9) Fujiki, M.; Koe, J. R. In *Silicon Based Polymers: The Science and Technology of their Synthesis and Applications*; Jones, R. G., Ando, W., Chojnowski, J., Eds.; Kluwer Academic Publishers: Dordrecht, The Netherlands, 2000; pp 643−665.

(10) Sandström, N.; Ottosson, H. *Chem.−Eur. J.* **2005**, *11*, 5067.

(11) Tibbelin, J.; Sandström, N.; Ottosson, H. *Silicon Chem.* **2007**, *3*, 165.

(12) Wiberg, K. B.; Connor, D. S.; Lampman, G. M. *Tetrahedron Lett.* **1964**, *5*, 531.

(13) Semmler, F. W.; Bartelt, K. *Ber. Dtsch. Chem. Ges.* **1907**, *40*, 4844.

(14) Casher, D. L.; Tsuji, H.; Sano, A.; Katkevics, M.; Toshimitsu, A.; Tamao, K.; Kubota, M.; Kobayashi, T.; Ottosson, H. C.; David, D. E.; Michl, J. *J. Phys. Chem. A* **2003**, *107*, 3559.

(15) (a) Piqueras, M. C.; Merchán, M.; Crespo, R.; Michl, J. *J. Phys. Chem. A* **2002**, *106*, 9868. (b) Crespo, R.; Merchán, M.; Michl, J. *J. Phys. Chem. A* **2000**, *104*, 8593.

(16) Piqueras, M. C.; Crespo, R.; Michl, J. *J. Phys. Chem.* **2003**, *107*, 4661.

(17) Becke, A. D. *J. Chem. Phys.* **1993**, *98*, 5648.

(18) Hariharan, P. C.; Pople, J. A. *Theor. Chim. Acta.* **1973**, *28*, 213.

(19) Kendall, R. A.; Dunning, T. H., Jr.; Harrison, R. J. *J. Chem. Phys.* **1992**, *96*, 6796.

(20) Frisch, M. J.; Trucks, G. W.; Schlegel, H. B.; Scuseria, G. E.; Robb, M. A.; Cheeseman, J. R.; Montgomery, Jr., J. A.; Vreven, T.; Kudin, K. N.; Burant, J. C.; Millam, J. M.; Iyengar, S. S.; Tomasi, J.; Barone, V.; Mennucci, B.; Cossi, M.; Scalmani, G.; Rega, N.; Petersson, G. A.; Nakatsuji, H.; Hada, M.; Ehara, M.; Toyota, K.; Fukuda, R.; Hasegawa, J.; Ishida, M.; Nakajima, T.; Honda, Y.; Kitao, O.; Nakai, H.; Klene, M.; Li, X.; Knox, J. E.; Hratchian, H. P.; Cross, J. B.; Bakken, V.; Adamo, C.; Jaramillo, J.; Gomperts, R.; Stratmann, R. E.; Yazyev, O.; Austin, A. J.; Cammi, R.; Pomelli, C.; Ochterski, J. W.; Ayala, P. Y.; Morokuma, K.; Voth, G. A.; Salvador, P.; Dannenberg, J. J.; Zakrzewski, V. G.; Dapprich, S.; Daniels, A. D.; Strain, M. C.; Farkas, O.; Malick, D. K.; Rabuck, A. D.; Raghavachari, K.; Foresman, J. B.; Ortiz, J. V.; Cui, Q.; Baboul, A. G.; Clifford, S.; Cioslowski, J.; Stefanov, B. B.; Liu, G.; Liashenko, A.; Piskorz, P.; Komaromi, I.; Martin, R. L.; Fox, D. J.; Keith, T.; Al-Laham, M. A.; Peng, C. Y.; Nanayakkara, A.; Challacombe, M.; Gill, P. M. W.; Johnson, B.; Chen, W.; Wong, M. W.; Gonzalez, C.; Pople, J. A. *Gaussian 03*, revision C.02; Gaussian, Inc., Wallingford CT, 2004.

(21) George, P.; Trachtman, M.; Bock, C. W.; Brett, A. M. *Tetrahedron* **1976**, *32*, 317.

(22) Widmark, P. O.; Persson, B. J.; Roos, B. O. *Theor. Chem. Acta.* **1991**, *79*, 419.

(23) Andersson, K.; Malmqvist, P. A.; Roos, B. O. *J. Chem. Phys.* **1992**, *96*, 1218.

(24) Roos, B. O.; Taylor, P. R.; Siegbahn, P. E. M. *Chem. Phys.* **1980**, *48*, 157.

(25) Finley, J.; Malmqvist, P. A.; Roos, B. O.; Serrano-Andrés, L. *Chem. Phys. Lett.* **1998**, *288*, 299.

(26) Piqueras, M. C.; Crespo, R.; Michl, J. *Mol. Phys.* **2001**, *100*, 747.

(27) Piqueras, M. C.; Michl, J.; Crespo, R. *Mol. Phys.* **2006**, *104*, 1107.

(28) Forsberg, N.; Malmqvist, P.-Å. *Chem. Phys. Lett.* **1997**, *274*, 196.

(29) Malmqvist, P.-Å.; Roos, B. O. *Chem. Phys. Lett.* **1989**, *155*, 189.

(30) Karlström, G., Lindh, R.; Malmqvist, P.-Å.; Roos, B. O.; Ryde, U.; Veryazov, V.; Widmark, P.-O.; Cossi, M.; Schimmelpfennig, B.; Neogrady, P.; Seijo, L. *Comput. Mater. Sci.* **2003**, *28*, 222.

(31) Niessen, W. von; Schirmer, J.; Cederbaum, L. S. *Comp. Phys. Rep.* **1984**, *1*, 57.

(32) Beagly, B.; Monaghan, J. J.; Hewitt, T. G. *J. Mol. Struct.* **1971**, *8*, 401.

(33) Iwamoto, T.; Yin, D.; Kabuto, Kira, M. *J. Am. Chem. Soc.* **2001**, *123*, 12730.

(34) (a) Wiberg, N.; Schuster, H.; Simon, A.; Peters, K. *Angew. Chem. Int., Ed. Engl.* **1986**, *25*, 79. (b) Wiberg, N.; Niedermayer, W.; Noth, H.; Kniezek, J.; Ponikwar, W.; Polborn, K. *Z. Naturforsch.* **2000**, *55b*, 389.

(35) Kaftory, M.; Kapon, M.; Botoshansky, M. In *The Chemistry of Organic Silicon Compounds*; Rappoport, Z., Apeloig, Y., Eds.; Wiley: Chichester, 1998; Vol. 2, p 181.